Model-Inversion-Based Fast Charging Control of Lithium-Ion Batteries Considering Parameter Uncertainty

Yao Cai

Technical Report No. 1111-111X
ISSN 3.1415-9265
This thesis has been prepared using LaTeX.

Department of Electrical Engineering
Chalmers University of Technology
SE-412 96 Gothenburg, Sweden
Phone: +46 (0)31 772 1000
www.chalmers.se

Printed by Chalmers Reproservice
Gothenburg, Sweden, August 2024

To my families

Abstract

The lithium-ion battery is a key technology for achieving sustainable mobility. However, due to its limited energy density, one of the main obstacles to replacing fossil-fueled vehicles with lithium-ion battery-powered electric vehicles is range anxiety. Ultra-fast charging is one way of resolving this issue. Unfortunately, simply increasing the charging current rates to reduce the charging time can lead to accelerated aging and shortened service life if the internal conditions of the battery cell are ignored. To achieve health-aware fast charging, an electrochemical model can provide valuable information for observing the internal states of batteries. A well-designed charging algorithm is needed to balance the trade-off between charging time and the rate of degradation. However, this is a challenging task due to uncertainties arising from various high-dimensional modeling and measurement errors.

This thesis investigates the influence of various uncertainties in designing the fast-charging control algorithms of lithium-ion batteries, such as current sensor bias, structural model differences, and errors in identified parameters. The study starts by spatially discretizing the pseudo two-dimensional (P2D) model, the most widely used electrochemical modeling framework for lithium-ion batteries. One key finding is that in the presence of parameter uncertainties, increasing the system order of the discretized model does not necessarily yield meaningful improvements. These uncertainties are often inherent due to difficulties in measurements or lack of clear physical interpretations.

To address the influence of parameter uncertainty during fast charging, a method for calculating a suitable safety margin to avoid lithium plating is developed by inverting the single particle model (SPM) of lithium-ion batteries. With knowledge of the range of parameter biases, the sensitivity of the safety margin with respect to these biases can be calculated, and the range of the safety margin can be determined. The minimum constant safety margin enabling lithium-plating-free fast charging is calculated based on this. An analysis shows that the required charging time is heavily dependent on the set safety margin. To achieve optimized performance, a method for calculating a time-varying safety margin is therefore developed, which speeds up the charging process by determining the maximum possible charging current based on the range of given parameter uncertainties at each time instant. Based on this

method, an online strategy is proposed to further reduce the charging time by adaptively updating the learned information about the uncertainties.

To conclude, this thesis contributes to the field by analyzing previously overlooked factors affecting aging-aware fast-charging design based on electrochemical models. Building on this analysis, methods to determine both constant and dynamic safety margins with online parameter uncertainty reduction are derived. The proposed methods ensure that shortened charging times can be achieved without inducing lithium plating, even under various model uncertainties, which is promising for future health-aware charging of electric vehicles.

Keywords: Lithium-ion battery, Electrochemical model, Parameter sensitivity analysis, Parameter identification, Safety margin

List of Publications

This thesis is based on the following publications:

[A] **Yao Cai**, Changfu Zou, Yang Li, and Torsten Wik, "Fast Charging Control of Lithium-Ion Batteries: Effects of Input, Model, and Parameter Uncertainties". Published in 2022 *European Control Conference (ECC)*, pp. 1647–1653, July 2022.

[B] **Yao Cai**, Yang Li, Torsten Wik , "Safety Margin for Li-Plating Free Fast-Charging of Li-Ion Batteries Considering Parameter Uncertainty". Accepted in 8th IEEE *Conference on Control Technology and Applications (CCTA)* Newcastle upon Tyne, 2024-08-21 - 2024-08-23.

[C] **Yao Cai**, Yang Li, Torsten Wik , "Dynamic Safety Margin with Parameter Identification for Li-Plating-Free Fast-Charging of Li-Ion Batteries". *Manuscript* for submission, July 2024.

Other publications by the author, not included in this thesis, are:

[D] Ze Zhang, **Yao Cai**, etc , "Collision-Free Trajectory Planning of Mobile Robots by Integrating Deep Reinforcement Learning and Model Predictive Control". Published in IEEE 19th International *Conference on Automation Science and Engineering (CASE)*, Auckland, New Zealand, 2023-08-26 - 2023-08-30.

Acknowledgments

I would like to express my deepest gratitude to my supervisors, Prof. Torsten Wik and Dr. Yang Li, for their patient support, guidance, and encouragement throughout this journey. Their expertise and insightful feedback have been invaluable in shaping this work, I feel very lucky to have had the opportunity to learn from them.

To my friends and colleagues, thank you for your encouragement and help. Your support has been instrumental in helping me navigate the challenges along the way. Special thanks to my friend Xinyuan Shao for being my friend.

Lastly, I am immensely grateful to my parents, whose love and unconditional support have been a source of strength and inspiration for me. Also, I want to extend a heartfelt thank you to my cat Lyapunov, for his companionship and healthy growth.

Thank you all for being an integral part of this endeavour.

Acronyms

P2D:	Pseudo Two-Dimensional
SPM:	Single Particle Model
EV:	Electric Vehicle
BMS:	Battery Management System
ECM:	Equivalent-Circuit Model
ABMS:	Advanced Battery Management System
SEI:	Solid Electrolyte Interphase
ROM:	Reduced-Order Model
PID:	Proportional-Integral-Derivative
MPC:	Model Predictive Control
OED:	Optimal Experiment Design
SOC:	State of Charge
PDAE:	Partial Differential-Algebraic Equation
EC:	Ethylene Carbonate
CV:	Constant Voltage
CP:	Constant Power
CCCV:	Constant Current Constant Voltage
FVM:	Finite Volume Method
RLS:	Recursive Least Square

Contents

Part I

Overview

CHAPTER 1

Introduction

1.1 Motivation

As climate change receives increasing global attention, attaining a sustainable and climate-neutral world has become a primary goal for the future. A key aspect of achieving this target is reducing emissions from on-road vehicles, which account for about one-quarter of the energy-related greenhouse gas emissions in the EU. This has pushed the current automotive industry to shift its focus towards zero-emission transport and highlights the importance of electric vehicles (EVs) [1].

Many carmakers, including Tesla, Volvo, and BYD, have already begun to manufacture pure battery-powered EVs. The annual global sales volume of EVs has increased from 17,000 to 3.24 million between 2010 and 2020, with a projected increase to 22.7 million by 2028, signifying a massive market expansion [2], [3]. Currently, almost all sold EVs adopt lithium-ion batteries due to their relatively high energy density, low self-discharge, wide temperature operating range, and reasonable price [4].

The battery management system (BMS) is one of the essential components of lithium-ion battery-powered EVs. Its main functions include monitoring battery states, balancing the charging and discharging processes, and ensuring that operations stay within specified constraints. For this reason, mathematical methods are required [5], [6]. Empirical battery models, such as equivalent-circuit models (ECMs), are commonly used in practice due to their simplicity and low computational requirements. However, these models are constructed using electrical circuit components by fitting the output voltage data to given input current excitations, without considering internal reactions and physical states. This limitation implies that they lack the ability to predict a cell's internal behaviors, which are directly related to battery health and safety. Without monitoring the battery's internal states, accelerated degradation and even safety issues can easily occur, particularly during the charging process. Relying on empirical models such as ECMs cannot ensure optimal battery usage, thus potentially shortening the battery lifespan significantly [7].

Considering the extensive use of lithium-ion batteries, there is a pressing need for advanced battery management systems (ABMSs). An ABMS can potentially monitor internal states related to battery degradation, such as lithium-ion concentrations, side-reaction overpotentials, and the thickness of the solid-electrolyte interphase (SEI) layer, which are typically unmeasurable due to sensor limitations. Observing these health-related states inside lithium-ion batteries is beyond the capabilities of ECMs. Consequently, electrochemical models have been introduced for ABMSs. Unlike empirical models, electrochemical models are physics-based and developed based on electrochemical principles governing internal dynamics and reactions. This enables prediction of the states inside the battery during the charging and discharging processes [8].

One of the most widely studied electrochemical models is the pseudo two-dimensional (P2D) model, which integrates mathematical descriptions of both macroscopic and microscopic behaviors of lithium-ion batteries. This enhances the model's ability to predict battery performance at different temporal and spatial scales. With the P2D model, closed-loop control and optimization-based methods can be designed to achieve health-aware fast charging [9], [10]. However, the P2D model is a system of partial differential-algebraic equations

(PDAEs) with a large number of parameters. Its complex structure imposes a heavy computational burden and challenges in parameter identification, making optimal control design intractable and real-time implementation impractical [11].

To address these challenges, efforts typically focus on two approaches. One approach is to simplify the electrochemical model by reducing the order of the P2D model while preserving its physical meaning [12], [13]. A well-known reduced-order model (ROM) is the single particle model (SPM), which assumes one layer of particles in each electrode and ignores the changes in lithium concentration in electrolyte. These simplifications significantly reduce the model complexity while retaining the ability to predict health-related phenomena such as lithium plating and the growth of the SEI layer. Furthermore, parameters of the SPM can be grouped to facilitate the design of real-time health-conscious fast-charging strategies [14].

In addition to simplifying models, advanced control methods have been proposed to make model based control numerically tractable. One promising optimization-free method is the model-inversion-based approach [15]. Unlike proportional-integral-derivative (PID) control [9], [16] and model predictive control (MPC) [17], [18], which require careful tuning of control parameters for different battery types and aging states, the model-inversion-based method computes analytical solutions for the optimal control input directly based on tracking goals, given that the model parameters are available. This approach significantly enhances computational efficiency, making it feasible for studies involving extensive simulations [15]. However, the effectiveness of the model-inversion-based method depends on the accuracy of the model parameters in generating reasonable control currents. Errors in the parameters can lead to deviations from the tracking goals, potentially causing accelerated battery degradation or even safety issues.

To deal with the main limitations of the model-inversion-based method, accurate parameterization is crucial but rather challenging. The difficulty arises primarily due to the complexity of electrochemical models. For instance, there are around one hundred parameters in the P2D model, most of which are difficult to measure directly, and many lack clear physical meanings despite being

derived from first principles. Even in a ROM with fewer parameters, not all can be straightforwardly obtained. These parameters can only be identified with carefully designed input excitations, an area that have recently been extensively investigated to improve the accuracy and reliability of the identified parameters [19], [20]. However, unidentifiability can arise due to structural errors in the model, insufficient experimental data, or noise, regardless of the methods used [21]. Therefore, before proceeding with parameter identification, it is important to check whether the parameters are identifiable, which can be achieved through parameter sensitivity analysis [3], [22]. Based on the results of parameter sensitivity analysis and optimal experiment design (OED), which utilizes the input's effects on parameter sensitivity, maximum parameter identifiability can be achieved [19], [23]. However, there will still be biases in the identified parameters, especially as a battery ages over its lifetime. Degradation-related parameters can change significantly over time, rendering initially identified parameters unsuitable for later use.

Another way to ensure health-conscious charging when applying the model-inversion-based control is to establish a safety margin for the tracking goal, to account for the impact of biased parameters. However, determining this safety margin often relies on the designer's experience due to the lack of rigorous methods in the literature.

Based on the aforementioned research challenges, this thesis work attempts to address the following main research problems in the area of electrochemical modelling and control of lithium-ion batteries:

- Sensitivity analysis of the P2D model parameters concerning the aging-related states
- Analytical calculation of the lithium-plating safety margin for the model-inversion-based charging strategy based on the SPM with grouped parameters

1.2 Thesis Contributions

Contributions of this thesis can be summarized as follows, as reported in the three appended papers:

1. The affecting factors when performing fast charging are studied. Three aspects of the effects are focused, including the input current bias, model size, and parameter uncertainties. This is done based on the P2D model, which includes sensitivity analysis not only on the outputs but also on the degradation states, such as the lithium-plating potential and the thickness of the SEI layer. (See Paper A)

2. A minimum constant safety margin is calculated to increase the charging speed without causing lithium-plating under inversion-based output tracking. This study is based on the SPM with grouped parameters, assuming known bias ranges in the model parameters. Through analytical calculations, a constant safety margin is determined that can prevent lithium-plating across all possible parameter combinations. (See Paper B)

3. An online dynamic safety margin with respect to the state of charge (SOC) is developed. When performing fast charging based on the SPM-inversion-based output tracking, a SOC-dependent safety margin can be calculated at every time instant. In addition, it is shown that the output voltage error can be approximated by a linear regression with the biases as unknown parameters. Consequently, a recursive linear least square estimation can be applied to estimate the model parameters. Employing this dynamic safety margin and parameter identification method, the model parameter bias ranges can be narrowed during Li-plating free fast-charging and the charging time can be significantly reduced compared to using the constant safety margin. (See Paper C)

1.3 Thesis Outline

In this thesis, Part I includes five chapters that are described in the following list:

- Chapter 1 provides the motivation and overall introduction of the thesis.
- Chapter 2 gives an overview of lithium-ion batteries and introduces various lithium-ion batteries models.
- Chapter 3 discusses some useful methods when performing fast charging,

including the parameter sensitivity analysis, the calculation of lithium plating safety margin, and parameter identification.

- Chapter 4 provides a summary of papers the thesis is based on.
- Chapter 5 gives concluding remarks and suggests directions for future research.

Part II includes the papers the thesis is built on.

CHAPTER 2

Lithium-Ion Battery Models

2.1 Lithium-Ion Batteries

Batteries play an extremely important role in the modern world as one of the most easy-to-use portable energy storage devices. In batteries, energy is stored in electrochemical forms and can be easily converted to electricity. While primary batteries cannot be recharged and are useless once they are depleted, many types of secondary batteries involve reversible chemical reactions, allowing them to be recharged multiple times. Among various types of secondary batteries, lithium-ion batteries have gradually become the most commonly used ones and today dominate the battery market for their outstanding characteristics. They are widely used as a rechargeable power supply in many mobile applications, ranging from portable electronic devices to road transport.

Why choose lithium-ion batteries

The lithium-ion battery offers a good balance between battery energy density and safety. Generally, a more active metal tends to have higher energy

density. However, higher activity also means greater instability in practice. In this aspect, the lithium-ion battery has been found to be a good trade-off between these two characteristics.

As shown in Fig. 2.1, compared to traditional batteries such as lead-acid and nickel-cadmium batteries, lithium-ion batteries have both high volumetric and gravimetric energy densities. Although metal-air batteries have higher energy density due to their air electrode, secondary metal-air batteries are still immature with materials and electrochemical issues [24].

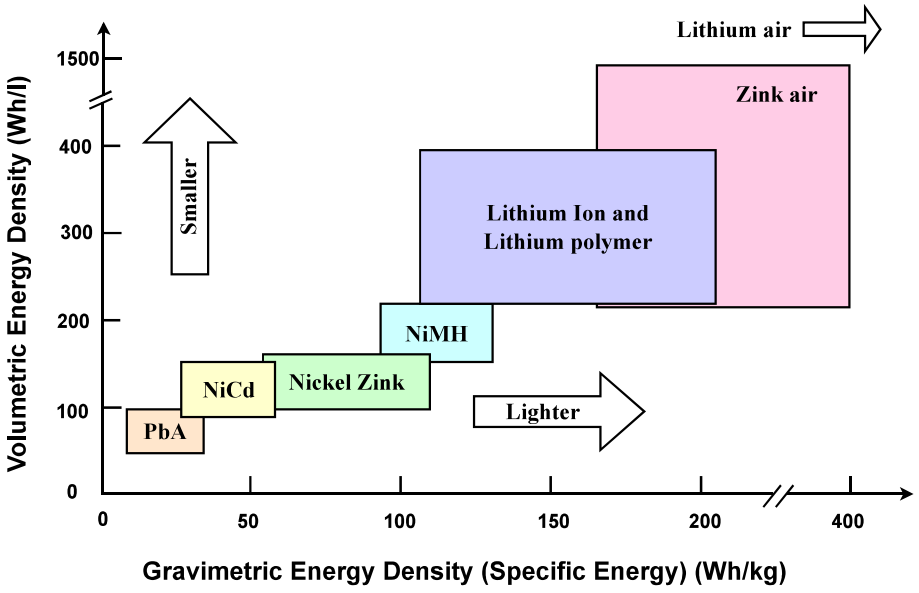

Figure 2.1: Energy density of different types of batteries (Redrawn from [24])

In addition, lithium-ion batteries have no memory effect and require minimal maintenance. Their low self-discharge rates and excellent fast charging capability have led to growing interest in related research topics [25].

Working principles

The working principle of lithium-ion batteries is based on the transfer of lithium ions between two electrodes. In a single lithium-ion battery cell, during discharging, lithium ions move from the negative electrode, through the

separator, to the positive electrode. Conversely, during charging, the lithium ions move in the opposite position, i.e., from the positive electrode, through the separator, to the negative electrode. The movement is driven by the potential difference between the positive and negative electrodes, enabling electrochemical conversion between stored electrochemical energy and electricity. However, during the battery lifetime, degradation can occur due to various mechanisms, such as the growth of the solid-electrolyte-interface (SEI) layer, lithium-plating, structural changes, electrolyte decomposition, and particle fracture. These degradation phenomena can manifest under normal operating conditions, resulting in capacity and power fade. Fast charging can further accelerate the degradation processes. Consequently, prolonging battery lifetime while achieving the most rapid charging has emerged as a critical research objective [26], [27].

2.2 Lithium-Ion Battery Models

Equivalent-circuit models

Empirical models focus solely on the battery input-output characteristics instead of the reactions and ion transport inside the battery. The most commonly used empirical models are the equivalent-circuit models (ECMs). ECMs utilize electrical elements such as capacitors, inductors, and resistors to construct a circuit that can reproduce voltage responses under given input current profiles. It is the state-of-the-art in battery management systems (BMSs) because of its simplicity. A first-order RC ECM is shown in Fig. 2.2.

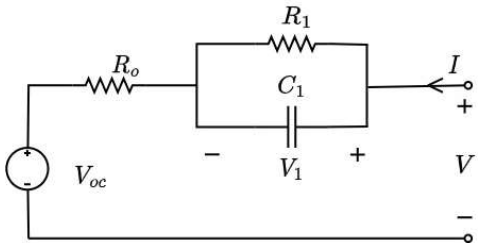

Figure 2.2: A first-order ECM.

The ECM shown in Fig. 2.2 has three parameters, R_o, R_1, and C_1. With V defined as the battery terminal voltage and I defined as the input current,

the equations of this ECM are given as [28], [29]:

$$\begin{aligned} \dot{V}_1(t) &= -\frac{V_1(t)}{R_1 C_1} + \frac{I(t)}{C_1}, \\ V(t) &= V_{\text{oc}}(Z) + R_o I(t) + V_1(t), \\ \text{SOC}(t) &= \text{SOC}(0) + \frac{1}{Q}\int_0^t I(\tau)d\tau, \end{aligned} \tag{2.1}$$

where t is the time index, $\text{SOC} \in [0, 1]$ is the state of charge, V_1 is the voltage of the parallel RC branch, V_{oc} is the open-circuit voltage, and Q is the capacity of the cell. Here, V_{oc} is a nonlinear function of the SOC, and a positive I indicates the cell is being charged. Although ECMs are simple to implement and widely used, the disadvantage of ECMs is also obvious: As an empirical input-output model, an ECM cannot describe the real process inside the battery, and consequently not the degradation mechanisms that are crucial during fast charging.

Electrochemical models

The electrochemical lithium-ion battery model addresses the drawbacks of ECMs. The probably most widely investigated electrochemical model of lithium-ion batteries in the literature, namely the P2D model, was first introduced by Newman, Doyle, and Fuller in the 1990s [30], [31]. Apart from its potentially higher accuracy compared to the ECMs, the first-principle model's predictive capability under various operating conditions and its ability to consider degradation mechanisms are particularly attractive. Despite these benefits, this electrochemical model has had limited practical implementation because of its complexity. Even considering nowadays' computational capabilities, implementing them in a vehicle BMS can be challenging.

The P2D model was developed based on the porous electrode theory and the concentrated solution theory, which describe the battery dynamics with a set of coupled partial differential-algebraic equations (PDAEs). The P2D model predicts the cell voltage response to an applied input current and provides spatially resolved internal potentials, lithium cation concentrations, and intercalated lithium concentrations. To reduce the computational load of the P2D model, many model reduction methods have been proposed to facilitate

implementation in control applications. The most mathematical nature is spatial discretization, which is also referred to as the method of lines. The simplest discretization is to take each electrode as one control volume. Combining this with the assumption of no electrolyte dynamics gives the most notable reduced-order model, the single particle model (SPM). Many research efforts have been built on the SPM and its extensions thanks to its computational efficiency, enabling real-time closed-loop control and optimization in advanced battery management systems (ABMSs).

In the following, a P2D model is described. A schematic diagram of the P2D model is shown in Fig. 2.3, where the thickness direction of the cell is regarded as the x-axis. The interface between the positive electrode and the positive current collector is defined as $x = 0$, and the interface between the negative electrode and the negative current collector is defined as $x = L$. Here, $L = L_p + L_s + L_n$, where L_p, L_s and L_n represent the thickness of the positive electrode, the separator and the negative electrode, respectively. The point immediately to the left of $x = L_p$ is denoted as $x = L_p^-$ and immediately to the right $x = L_p^+$, and a similar notation is used for the point $x = L_p + L_s$. The current collectors are not modelled in detail in this work, and only the positive electrode, the separator, and the negative electrode will be described in the governing equations. In the following, for the concentrations and the electrical potentials, the first index $\{s, e\}$ of the subscript represents solid material or electrolyte, and the second index $i \in \{p, sep, n\}$ of the subscript represents the domain of positive electrode, separator, or negative electrode. For other symbols, index $i \in \{p, sep, n\}$ of the subscript represents the domain of the positive electrode, separator, or negative electrode. The governing equations of the different parts are given in accordance with [32], [33] and the meanings and units of the symbols used in the model are listed in Table 2.1.

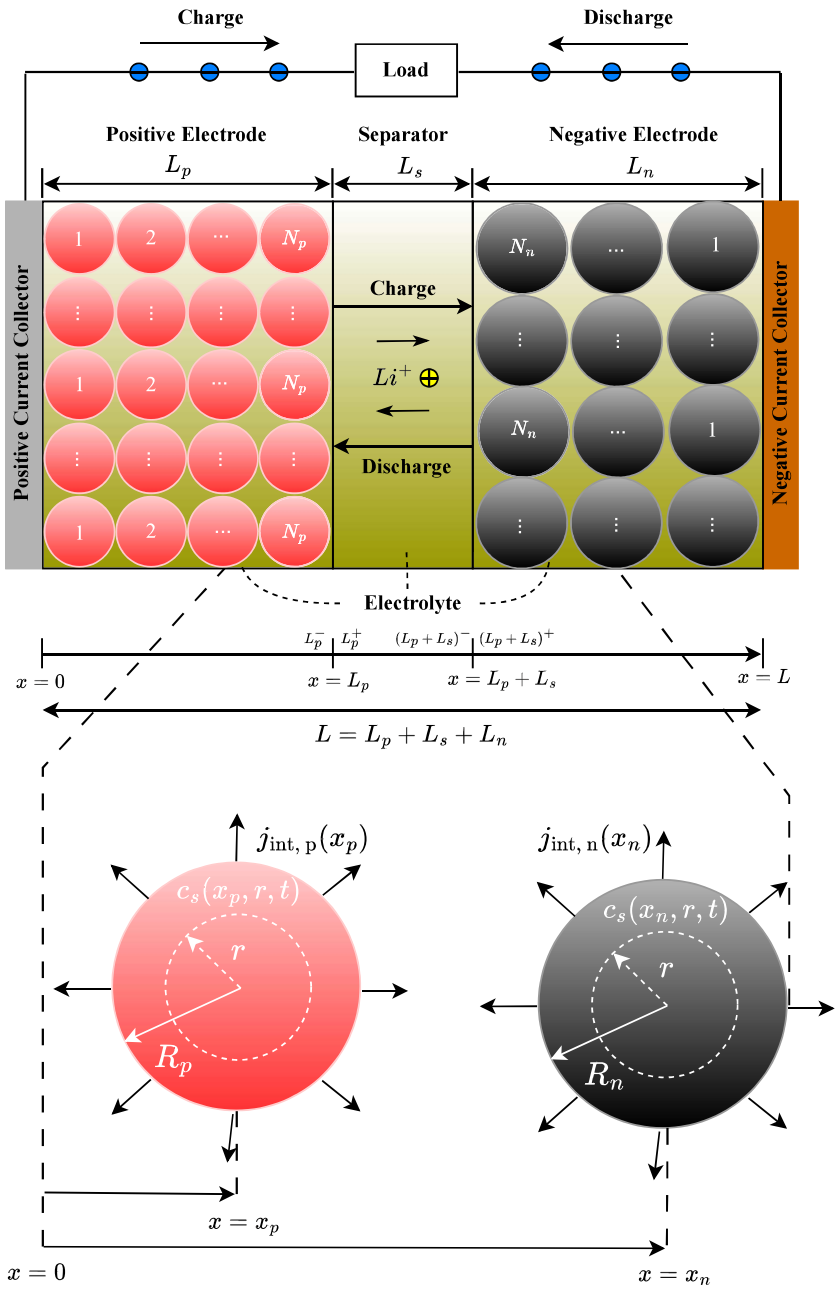

Figure 2.3: 1D schematic of a Li-ion battery cell with N_p layers of particles in the positive electrode and N_n layers of particles in the negative electrode. From left to right, the three compartments represent the positive electrode, the separator, and the negative electrode, respectively.

Table 2.1: List of symbols used in P2D model

Symbol	Physical Meaning	Unit
Φ_s	solid-phase potential	V
Φ_e	electrolyte potential	V
c_s	solid-phase concentration	$\mathrm{mol \cdot m^{-3}}$
c_s^{avg}	volume-averaged solid-phase concentration	$\mathrm{mol \cdot m^{-3}}$
c_s^{max}	theoretical maximum solid-phase concentration	$\mathrm{mol \cdot m^{-3}}$
c^{ss}	surface concentration of solid-particle	$\mathrm{mol \cdot m^{-3}}$
c_s^{diff}	concentration difference between c_s^{avg} andc^{ss}	$\mathrm{mol \cdot m^{-3}}$
c_{EC}^0	concentration of EC in the bulk electrolyte	$\mathrm{mol \cdot m^{-3}}$
c_e	electrolyte concentration	$\mathrm{mol \cdot m^{-3}}$
c_e^0	initial electrolyte concentration	$\mathrm{mol \cdot m^{-3}}$
j_{tot}	total molar flux	$\mathrm{mol \cdot m^{-2} \cdot s^{-1}}$
j_{int}	intercalation molar flux	$\mathrm{mol \cdot m^{-2} \cdot s^{-1}}$
j_{SEI}	SEI molar flux	$\mathrm{mol \cdot m^{-2} \cdot s^{-1}}$
j_{LiP}	lithium plating molar flux	$\mathrm{mol \cdot m^{-2} \cdot s^{-1}}$
i_0	exchange current density	$\mathrm{A \cdot m^{-2}}$
η_{int}	activation overpotential for intercalation	V
η_{LiP}	activation overpotential for lithium plating	V
U	equilibrium potential of the electrode	V
D_s	solid-phase diffusion coefficient at reference temperature	$\mathrm{m^2 \cdot s^{-1}}$
D_e	electrolyte diffusion coefficient	$\mathrm{m^2 \cdot s^{-1}}$
D_e^{eff}	effective electrolyte diffusion coefficient	$\mathrm{m^2 \cdot s^{-1}}$
D_{EC}	diffusivity of EC	$\mathrm{m^2 \cdot s^{-1}}$
R_s	radius of the solid-phase particle	m
a	specific surface area of electrode ($= 3\varepsilon_s/R_s$)	$\mathrm{m^{-1}}$
ε_s	volume fraction of the solid phase	-
ε_e	porosity or volume fraction of the electrolyte	-
σ	solid-phase conductivity	$\mathrm{S \cdot m^{-1}}$
κ	electrolyte (ionic) conductivity	$\mathrm{S \cdot m^{-1}}$
σ^{eff}	effective solid-phase conductivity	$\mathrm{S \cdot m^{-1}}$
κ^{eff}	effective electrolyte (ionic) conductivity	$\mathrm{S \cdot m^{-1}}$
k^{eff}	effective reaction rate constant	$\mathrm{A \cdot m^{2.5} \cdot mol^{-1.5}}$
k	reaction rate constant at reference temperature	$\mathrm{A \cdot m^{2.5} \cdot mol^{-1.5}}$
L	thickness of a domain	m
R_{film}	SEI film resistance	$\mathrm{\Omega \cdot m^2}$
r_{col}	resistance of the current collector	$\mathrm{\Omega \cdot m^2}$
δ_C	thickness of the surface film	m
F	Faraday constant	$\mathrm{s \cdot A \cdot mol^{-1}}$
T	cell temperature	K
R	universal gas constant	$\mathrm{J \cdot K^{-1} \cdot mol^{-1}}$
t_+^0	transference number	-
A	electrode plate area	$\mathrm{m^2}$
r	radial position across a spherical particle	m
x	position across cell	m
t	time	s
brugg	Bruggeman's coefficient	-
i_{app}	applied current density	$\mathrm{A \cdot m^{-2}}$
I	applied current	A
α_a	anodic charge transfer coefficient	-
α_c	cathodic charge transfer coefficient	-

Solid phase

In the solid active material of the two electrodes, the lithium-ion concentration is described by Fick's law of diffusion along the r-direction

$$\frac{\partial c_{s,i}(x,r,t)}{\partial t} = \frac{1}{r^2}\frac{\partial}{\partial r}\left(D_{s,i}r^2\frac{\partial c_{s,i}(x,r,t)}{\partial r}\right), \tag{2.2}$$

where $c_{s,i}$ is the lithium-ion concentration in the solid active material, $D_{s,i}$ is the diffusion coefficient for the solid particle, and r denotes the radial distance in a solid particle at the microscale while x indicates the position at the macroscale. The corresponding boundary conditions are

$$\left.\frac{\partial c_{s,i}(x,r,t)}{\partial r}\right|_{r=0} = 0, \quad \left.\frac{\partial c_{s,i}(x,r,t)}{\partial r}\right|_{r=R_{s,i}} = -\frac{j_{\text{int},i}(x,t)}{D_{s,i}}, \tag{2.3}$$

where $j_{\text{int},i}$ is the intercalation molar flux of lithium-ions through the particle surface and $R_{s,i}$ represents the radius of the solid particles. These boundary conditions reflect the assumptions that at the surface of the particles, the derivatives of $c_{s,i}$ with respect to the radius are proportional to $j_{\text{int},i}$, and in the centre of the particle, the derivatives are zero because of symmetry (no flux).

The default initial condition is given by

$$c_{s,i}(x,r,0) = c_{s,i}^{\text{avg},0}, \tag{2.4}$$

where $c_{s,i}^{\text{avg},0}$ is the electrode volume-averaged concentration when the battery is in a steady state.

Electrolyte phase

In the electrolyte, the lithium-ion transport can be described by

$$\varepsilon_{e,i}\frac{\partial c_{e,i}(x,t)}{\partial t} = \frac{\partial}{\partial x}\left(D_{e,i}^{\text{eff}}\frac{\partial c_{e,i}(x,t)}{\partial x}\right) + a_i\left(1-t_+^0\right)j_{\text{tot},i}(x,t), \tag{2.5}$$

where $c_{e,i}(x,t)$ is the electrolyte lithium-ion concentration in domain i. $D_{e,i}^{\text{eff}}$ is the effective diffusion coefficient of the electrolyte and can be calculated by $D_{e,i}^{\text{eff}} = D_{e,i}\varepsilon_{e,i}^{\text{brugg}_i}$, where $D_{e,i}$ is the electrolyte diffusion coefficient in domain

i, brugg_i is the Bruggeman's coefficient in domain i, and $\varepsilon_{e,i}$ is the porosity in domain i. The effective electrolyte diffusion coefficient is used for compensating the tortuous path that the lithium ions go across the electrolyte. Here, $j_{\text{tot},i}$ is the total molar flux that considers the intercalation, which consists of the intercalation molar flux $j_{\text{int},i}$ and the side-reaction molar flux that will be discussed more in later sections.

For the separator, since there are no chemical reactions, the molar flux $j_{\text{tot},i}$ is considered zero and thus, the above equation needs to be modified by removing the second term on the right-hand side.

No electrolyte flux exists at the boundaries of the electrodes, the boundary conditions at the interfaces of the current collectors and the electrodes are

$$-D_{e,p}^{\text{eff}} \frac{\partial c_{e,p}}{\partial x}\bigg|_{x=0} = -D_{e,n}^{\text{eff}} \frac{\partial c_{e,n}}{\partial x}\bigg|_{x=L} = 0. \tag{2.6}$$

Also, on both sides of the interfaces of the electrodes and the separator, the concentration $c_{e,i}$ and their derivatives should be consistent. The boundary conditions at the electrodes and separator interfaces are therefore

$$-D_{e,p}^{\text{eff}} \frac{\partial c_{e,p}(x,t)}{\partial x}\bigg|_{x=L_p^-} = -D_{e,sep}^{\text{eff}} \frac{\partial c_{e,sep}(x,t)}{\partial x}\bigg|_{x=L_p^+} \tag{2.7}$$

$$-D_{e,sep}^{\text{eff}} \frac{\partial c_{e,sep}(x,t)}{\partial x}\bigg|_{x=(L_p+L_s)^-} = -D_{e,n}^{\text{eff}} \frac{\partial c_{e,n}(x,t)}{\partial x}\bigg|_{x=(L_p+L_s)^+} \tag{2.8}$$

$$c_{e,p}(x,t)|_{x=L_p^-} = c_{e,sep}(x,t)|_{x=L_p^+} \tag{2.9}$$

$$c_{e,s}(x,t)|_{x=(L_p+L_s)^-} = c_{e,n}(x,t)|_{x=(L_p+L_s)^+}. \tag{2.10}$$

An initial condition should naturally also be satisfied, i.e.

$$c_{e,i}(x,0) = c_e^0. \tag{2.11}$$

Electrical potential

The potential $\Phi_{s,i}$ in the solid phase of each electrode can be described by Ohm's law where $\sigma_i^{\text{eff}} = \varepsilon_{s,i}\sigma$ is the effective electronic conductivity of the

porous electrode and σ is the conductivity of the solid material. This gives

$$\sigma_i^{\text{eff}} \frac{\partial^2 \Phi_{s,i}(x,t)}{\partial x^2} = a_i F j_{\text{tot},i}(x,t), \tag{2.12}$$

with the boundary conditions at the current collectors being that the derivatives of $\Phi_{s,i}$ are proportional to the applied current density i_{app}, which is derived from the fact that the electrical current through the solid equals the total current entering or exiting the cell, together with that there is no electron flux at the interface of the electrode and the separator because there are no conductive solids in the separator. The boundary conditions are given as

$$-\sigma_p^{\text{eff}} \frac{\partial \Phi_{s,p}}{\partial x}\bigg|_{x=0} = -\sigma_n^{\text{eff}} \frac{\partial \Phi_{s,n}}{\partial x}\bigg|_{x=L} = i_{\text{app}} \tag{2.13}$$

$$-\sigma_p^{\text{eff}} \frac{\partial \Phi_{s,p}}{\partial x}\bigg|_{x=L_p} = -\sigma_n^{\text{eff}} \frac{\partial \Phi_{s,n}}{\partial x}\bigg|_{x=L_p+L_s} = 0. \tag{2.14}$$

The potential in the electrolyte phase is given by

$$a_i F j_{\text{tot},i}(x,t) = -\frac{\partial}{\partial x}\left[\kappa_i^{\text{eff}} \frac{\partial \Phi_{e,i}(x,t)}{\partial x} + \kappa_i^{\text{eff}} \frac{2(t_+^0 - 1)RT}{F} \frac{\partial \ln c_{e,i}(x,t)}{\partial x}\right], \tag{2.15}$$

where $\kappa_i^{\text{eff}} = \varepsilon_e \kappa_i$ is the effective ionic conductivity and T is the temperature. Since only potential differences are measurable, $\Phi_{e,n}$ can be set to zero at the interface of the anode and its current collector. At both interfaces of the electrodes and their current collectors the derivatives of $\Phi_{e,i}$ are set to zero for physical constraints. In addition, the derivatives of $\Phi_{e,i}$ are equal when crossing the interfaces of the electrodes and the separators. Overall, the boundary conditions are

$$-\kappa_p^{\text{eff}} \frac{\partial \Phi_{e,p}}{\partial x}\bigg|_{x=0} = -\kappa_n^{\text{eff}} \frac{\partial \Phi_{e,n}}{\partial x}\bigg|_{x=L} = \Phi_{e,n}|_{x=0} = 0 \tag{2.16}$$

$$-\kappa_p^{\text{eff}} \frac{\partial \Phi_{e,p}}{\partial x}\bigg|_{x=L_p^-} = -\kappa_{sep}^{\text{eff}} \frac{\partial \Phi_{e,sep}}{\partial x}\bigg|_{x=L_p^+} \tag{2.17}$$

$$-\kappa_{sep}^{\text{eff}} \frac{\partial \Phi_{e,sep}}{\partial x}\bigg|_{x=\left(L_p+L_s\right)^-} = -\kappa_n^{\text{eff}} \frac{\partial \Phi_{e,n}}{\partial x}\bigg|_{x=\left(L_p+L_s\right)^+}. \tag{2.18}$$

Butler–Volmer kinetics

The Butler–Volmer equation is an algebraic equation that couples the above PDEs. It describes the relationship between the intercalation molar flux,

concentrations, and overpotential according to

$$j_{\text{int},i}(x,t) = \frac{i_{0,i}}{F}\left[\exp\left(\frac{\alpha_a F \eta_{\text{int},i}(x,t)}{RT}\right) - \exp\left(-\frac{\alpha_c F \eta_{\text{int},i}(x,t)}{RT}\right)\right]. \tag{2.19}$$

Equation (2.19) works for the two electrodes and in the separator $j_{\text{int},i}$ is assumed to be zero since there is no solid phase in the separator domain. In (2.19), i_0 is the exchange current density, given by

$$i_{0,i} = k_i^{\text{eff}} F c_{e,i}(x,t)^{\alpha_a} \left(c_{s,i}^{\max} - c_i^{\text{ss}}(x,t)\right)^{\alpha_a} c_i^{\text{ss}}(x,t)^{\alpha_c}, \tag{2.20}$$

and η_{int} is the surface overpotential and is given by

$$\eta_{\text{int},i}(x,t) = \Phi_{s,i}(x,t) - \Phi_{e,i}(x,t) - F R_{\text{film},i} j_{\text{tot},i}(x,t) - U_i, \tag{2.21}$$

where U_i is the equilibrium potential of the lithium intercalation, $R_{\text{film},i}$ is the surface film resistance, and k_i^{eff} is the effective reaction rate constant. Usually, it is assumed that $\alpha_a = \alpha_c = 0.5$, and then (2.19) becomes

$$j_{\text{int},i}(x,t) = 2k_i^{\text{eff}} \sqrt{c_{e,i}(x,t)\left(c_{s,i}^{\max} - c_i^{\text{ss}}(x,t)\right) c_i^{\text{ss}}(x,t)} \sinh\left[\frac{0.5F}{RT}\eta_{\text{int}}(x,t)\right]. \tag{2.22}$$

Terminal voltage and SOC

The terminal voltage is given by

$$V(t) = \Phi_{s,p}(x,t)|_{x=0} - \Phi_{s,n}(x,t)|_{x=L} + r_{\text{col}} i_{\text{app}}, \tag{2.23}$$

where r_{col} is the resistance of the current collector per square meter, and i_{app} is the applied current density, defined as positive for charging. In this work r_{col} is taken as zero. Thus, V is calculated by

$$V(t) = \Phi_{s,p}(x,t)|_{x=0} - \Phi_{s,n}(x,t)|_{x=L}. \tag{2.24}$$

The bulk SOC is the average utilization of the entire electrode and is often used as an indicator of available energy in the cell [34]. In the positive and negative electrode, their bulk SOC can be represented as (2.25) and (2.26), respectively.

$$\begin{aligned} \mathrm{SOC}_p(t) &\triangleq \frac{3}{L_p \left(R_{s,p}\right)^3 c_{s,p}^{\max}} \int_0^{L_p} \int_0^{R_{s,p}} r^2 c_{s,p}(x,r,t) dr dx \\ &= \frac{1}{L_p c_{s,p}^{\max}} \int_0^{L_p} c_{s,p}^{\mathrm{avg}}(x,t) dx \end{aligned} \tag{2.25}$$

$$\begin{aligned} \mathrm{SOC}_n(t) &\triangleq \frac{3}{L_n \left(R_{s,n}\right)^3 c_{s,n}^{\max}} \int_{L_p+L_s}^{L} \int_0^{R_{s,n}} r^2 c_{s,n}(x,r,t) dr dx \\ &= \frac{1}{L_n c_{s,n}^{\max}} \int_{L_p+L_s}^{L} c_{s,n}^{\mathrm{avg}}(x,t) dx. \end{aligned} \tag{2.26}$$

Since SOC_p and SOC_n are directly related to each other, conventionally $\mathrm{SOC} = \mathrm{SOC}_n$ when referring to SOC.

Side Reactions

The degradation of the battery due to side reactions can be considered within the P2D modelling framework [33]. As mentioned earlier, the intercalation molar flux $j_{\mathrm{int},i}$ is only one part of the total molar flux $j_{\mathrm{tot},i}$. The rest is attributed to side reactions, including the SEI molar flux $j_{\mathrm{SEI},i}$ and the lithium plating molar flux $j_{\mathrm{LiP},i}$. In the following side reaction equations, the index i that indicates the domain is dropped for brevity, as these side reactions occur only in the negative electrode. It is assumed that the SEI is formed by the reaction between ethylene carbonate (EC) and lithium ions, generating lithium ethylene dicarbonate. First, the molar flux j_{SEI} associated with SEI side reactions can be calculated as

$$j_{\mathrm{SEI}} = -k_{0,\mathrm{SEI}} c_{\mathrm{EC}}^{\mathrm{ss}} \exp\left(-\frac{\alpha_{c,\mathrm{SEI}} F}{RT} \eta_{\mathrm{SEI}}\right), \tag{2.27}$$

with

$$\eta_{\mathrm{SEI}} = \Phi_s - \Phi_e - F R_{\mathrm{film}} j_{\mathrm{tot}} - U_{\mathrm{SEI}}, \tag{2.28}$$

where $k_{0,\mathrm{SEI}}$ is a kinetic rate constant, η_{SEI} is the overpotential, and U_{SEI} is the equilibrium potential of SEI formation reaction. $c_{\mathrm{EC}}^{\mathrm{ss}}$ is the concentration of EC on the surface of graphite, which is calculated based on the mass

conservation of EC:

$$-D_{\mathrm{EC}}\frac{c_{\mathrm{EC}}^{\mathrm{ss}}-c_{\mathrm{EC}}^{0}}{\delta_{\mathrm{film}}}=-j_{\mathrm{SEI}}, \tag{2.29}$$

where D_{EC} is the diffusivity of EC, c_{EC}^{0} is the concentration of EC in the bulk electrolyte, and δ_{film} is the thickness of the surface film. The left-hand side of (2.29) represents the diffusive flux of EC across the film, and the right-hand side denotes the consumption rate of EC.

Lithium plating is assumed to be irreversible in this model. That is, the stripping of plated lithium in the subsequent discharge process is neglected. As such, the following cathodic Tafel expression is used to calculate the transfer molar flux of the lithium deposition reaction:

$$j_{\mathrm{LiP}}=-\frac{i_{0,\mathrm{LiP}}}{F}\exp\left(-\frac{\alpha_{c,\mathrm{LiP}}F}{RT}\eta_{\mathrm{LiP}}\right),\quad\text{when}\quad\eta_{\mathrm{LiP}}<0, \tag{2.30}$$

where η_{LiP} is the lithium-plating overpotential, calculated by

$$\eta_{\mathrm{LiP}}=\Phi_s-\Phi_e-FR_{\mathrm{film}}j_{\mathrm{tot}}, \tag{2.31}$$

and $i_{0,\mathrm{LiP}}$ is the exchange current density of lithium deposition, which is treated as a fitting parameter in the present model due to the lack of reliable experiment data. Equation (2.30) indicates that lithium plating only occurs when η_{LiP} is below zero. j_{LiP} is considered as zero when $\eta_{\mathrm{LiP}}\geq 0$.

2.3 Reduced-Order Electrochemical Model

Solving a full P2D model requires significant programming and computational efforts making it unfit to run online. A reduced-order model (ROM) is therefore very useful when performing real-time control and or conducting huge numbers of long simulations. There are many ROM techniques in mathematics, though when it comes to P2D models there are four main categories of control-oriented methods that are applied. They are spatial discretization, function approximation, frequency domain approximation, and simplified physics/spatial lumping [35]. In this work, all four techniques are applied for P2D model simplification.

Reformulate Solid-Phase Diffusion Equation

Polynomial approximation

Before applying any method of lines along the x-dimension, it is conventional to reformulate (2.2). The diffusion inside the solid particles is described by (2.2) and many approaches have been adopted to simplify it. One commonly used method is to assume the spatial profile of the concentration is a quadratic function with respect to the radial position r. Equations (2.2) and (2.3) can then be simplified by using only the volume-averaged concentration $c_{s,i}^{\text{avg}}(x,t)$ and the surface concentration $c_i^{\text{ss}}(x,t)$ of the solid particles. This method is regarded as the two-parameter polynomial approximation [32], [36] in the literature, and the resulting model is given by

$$\frac{\partial c_{s,i}^{\text{avg}}(x,t)}{\partial t} = -\frac{3}{R_{s,i}} j_{\text{int},i}(x,t) \tag{2.32}$$

$$c_i^{\text{ss}}(x,t) = c_{s,i}^{\text{avg}}(x,t) - \frac{R_{s,i}}{5D_{s,i}} j_{\text{int},i}(x,t). \tag{2.33}$$

If the concentration profile is assumed to be a quadratic function with only even terms, the resulting three-parameter polynomial approximation leads to a 2nd-order model:

$$\frac{\partial c_{s,i}^{\text{avg}}(x,t)}{\partial t} = -\frac{3}{R_{s,i}} j_{\text{int},i}(x,t) \tag{2.34}$$

$$\frac{\partial q_i(x,t)}{\partial t} = -\frac{30D_{s,i}}{R_{s,i}^2} q_i(x,t) - \frac{45}{2R_{s,i}^2} j_{\text{int},i}(x,t) \tag{2.35}$$

$$c_i^{\text{ss}}(x,t) = c_{s,i}^{\text{avg}}(x,t) + 8R_{s,i} q_i(x,t) - \frac{R_{s,i}}{35D_{s,i}} j_{\text{int},i}(x,t), \tag{2.36}$$

where the physical meaning of the second state variable q_i is the concentration flux.

Padé Approximation

Instead of approximating the solid diffusion equation with the sum of different orders of polynomial combinations, Padé approximation works as a frequency domain method. Compared to the polynomial approximation, Padé approximation has better convergence properties and higher accuracy with the same order of polynomials [37].

Taking the Laplace transform of (2.2) and (2.3), one can obtain the following transcendental transfer function [35]

$$G_s(s) = \frac{c_i^{\text{ss}}(x,s)}{j_{\text{int},i}(x,s)} = \frac{R_{s,i}}{D_{s,i}} \frac{\tanh\left(R_{s,i}\sqrt{s/D_{s,i}}\right)}{\tanh\left(R_{s,i}\sqrt{s/D_{s,i}}\right) - R_{s,i}\sqrt{s/D_{s,i}}}. \tag{2.37}$$

For n-th order Padé approximation, the above transcendental transfer function is approximated using a rational transfer function

$$G_s(s) \approx P_s(s) = \frac{a_0 + a_1 s + \cdots + a_{n-1}s^{n-1}}{s(1 + b_2 s + \cdots + b_n s^{n-1})}. \tag{2.38}$$

To obtain the coefficient a_i $(i = 0, 1, \cdots, n-1)$ and b_j $(j = 2, 3, \cdots, n)$, we calculate the zeroth to $(2n-1)$th derivatives of $G_s(s)$ and $P_s(s)$ with respect to the complex frequency index s, and obtain $2n$ nonlinear equations, i.e.,

$$\frac{d^k G_s(s)}{ds^k} = \frac{d^k P_s(s)}{ds^k}, \quad \forall k \in \{0, 1, \cdots, 2n-1\}. \tag{2.39}$$

In this work, for simplicity we only consider the 2nd-order Padé approximation:

$$P_s(s) = -\frac{\frac{3}{R_{s,i}} + \frac{2R_{s,i}}{7D_{s,i}}s}{s + \frac{R_{s,i}^2}{35D_{s,i}}s^2} = -\frac{3}{R_{s,i}s} - \frac{\frac{R_{s,i}}{5D_{s,i}}}{1 + \frac{R_{s,i}^2}{35D_{s,i}}s}. \tag{2.40}$$

The corresponding state-space model is given by

$$\begin{aligned}
\frac{\partial c_{s,i}^{\text{avg}}(x,t)}{\partial t} &= -\frac{3}{R_{s,i}} j_{\text{int},i}(x,t) \\
\frac{\partial c_{s,i}^{\text{diff}}(x,t)}{\partial t} &= -\frac{35D_{s,i}}{R_{s,i}^2} c_{s,i}^{\text{diff}}(x,t) - \frac{7}{R_{s,i}} j_{\text{int},i}(x,t) \\
c_i^{\text{ss}}(x,t) &= c_{s,i}^{\text{avg}}(x,t) + c_{s,i}^{\text{diff}}(x,t).
\end{aligned} \tag{2.41}$$

Discretized Governing Equations

By performing a two-parameter polynomial approximation on the solid-phase diffusion equation, all the unknowns are functions of time t and x which is the direction in the thickness of the cell. Apply the finite volume method (FVM)

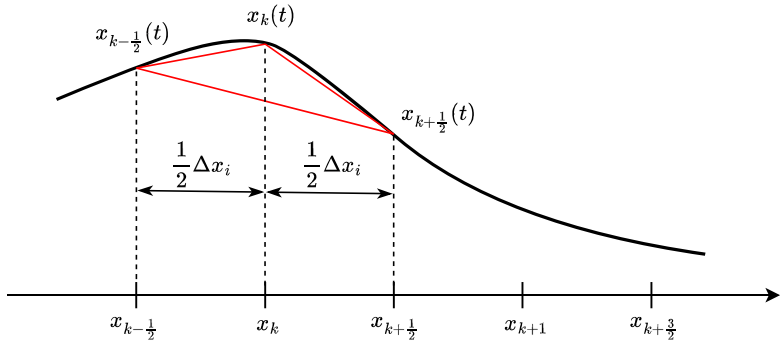

Figure 2.4: One-dimensional finite volume mesh.

on the reformulated P2D, by subdividing the positive electrode, the separator, and the negative electrode into N_p, N_s, and N_n, respectively, non-overlapping control volumes, where each control volume has a geometrically centered node. The width of every control volume is $\Delta x_i = L_i/N_i, i \in \{p, s, n\}$. The centre of the k-*th* volume is denoted as x_k and spans the interval $[x_{k-\frac{1}{2}}; x_{k+\frac{1}{2}}]$ as shown in Fig. 2.4. The resulting set of discretized governing equations are given in Table 2.2. The symbols with a bar above are the volume-averaged values, and $\bar{\Phi}_{e,\text{end}} = 0$ is the averaged electrolyte potential in the last control volume. Within reasonable limits, the larger N_p, N_s and N_n are, the higher the model accuracy, but at the price of an increased computational burden.

Table 2.2: FVM P2D equations

Positive and negative Electrodes, $i \in \{p, n\}$	Boundary conditions
$\epsilon_{e,i} \frac{\partial \bar{c}_{e,i,k}(t)}{\partial t} = \frac{1}{\Delta x_i} \left[D_{e,i}^{\text{eff}} \frac{\partial c_{e,i}(x,t)}{\partial x} \right] \Big\vert_{x_{k-\frac{1}{2}}}^{x_{k+\frac{1}{2}}} + a_i \left(1 - t_+^0\right) \bar{j}_{i,k}(t)$	$-D_{e,i}^{\text{eff}} \frac{\partial c_{e,i}(x,t)}{\partial x} \Big\vert_{x=0,L} = 0.$
$\frac{\partial \bar{c}_{s,i}^{\text{avg}}(t)}{\partial t} = -3 \frac{j_{i,k}(t)}{R_{s,i}}$	
$\bar{c}_i^{\text{ss}}(t) - \bar{c}_{s,i}^{\text{avg}}(t) = -\frac{R_{s,i}}{D_{s,i}^{\text{eff}}} \frac{\bar{j}_{i,k}(t)}{5}$	
$\left[\sigma_{\text{eff},i} \frac{\partial \Phi_{s,i}(x,t)}{\partial x} \right] \Big\vert_{x_{k-\frac{1}{2}}}^{x_{k+\frac{1}{2}}} = a_i F \bar{j}_{i,k}(t) \Delta x_i$	$\left[\sigma_i^{\text{eff}} \frac{\partial \Phi_{s,i}}{\partial x} \right] \Big\vert_{x=0,L} = -i_{\text{app}}$
	$\frac{\partial \Phi_{s,i}(x,t)}{\partial x} \Big\vert_{x=L_p, L_p+L_s} = 0$
$\left[\kappa_i^{\text{eff}} \frac{\partial \Phi_{e,i}(x,t)}{\partial x} \right] \Big\vert_{x_{k-\frac{1}{2}}}^{x_{k+\frac{1}{2}}} - \left[\kappa_i^{\text{eff}} \frac{2(1-t_+^0)RT}{F} \frac{\partial \ln c_{e,i}(x,t)}{\partial x} \right] \Big\vert_{x_{k-\frac{1}{2}}}^{x_{k+\frac{1}{2}}} = \Delta x_i a_i F \bar{j}_{i,k}(t)$	$\frac{\partial \Phi_{e,i}(x,t)}{\partial x} \Big\vert_{x=0} = 0$
	$\bar{\Phi}_{e,\text{ end}} = 0$
$\bar{j}_{i,k}(t) = 2k_i^{\text{eff}} \sqrt{\bar{c}_{e,i,k}(t) \left(c_{s,i}^{\max} - \bar{c}_{i,k}^{ss}(t)\right) \bar{c}_{i,k}^{ss}(t)} \sinh \left[\frac{0.5R}{FT} \bar{\eta}_{i,k}(t) \right]$	
$\bar{\eta}_{i,k}(t) = \bar{\Phi}_{s,i,k}(t) - \bar{\Phi}_{e,i,k}(t) - \bar{U}_{i,k}$	

Separator, $i = s$
$\varepsilon_{e,i} \frac{\partial \bar{c}_{e,i}(t)}{\partial t} = \frac{1}{\Delta x_i} \left[D_{e,i}^{\text{eff}} \frac{\partial c_{e,i}(x,t)}{\partial x} \right] \Big\vert_{x_{k-\frac{1}{2}}}^{x_{k+\frac{1}{2}}}$
$\left[\kappa_i^{\text{eff}} \frac{\partial \Phi_{e,i}(x,t)}{\partial x} \right] \Big\vert_{x_{k-\frac{1}{2}}}^{x_{k+\frac{1}{2}}} - \left[\kappa_i^{\text{eff}} \frac{2(1-t_+^0)RT}{F} \frac{\partial \ln c_{e,i}(x,t)}{\partial x} \right] \Big\vert_{x_{k-\frac{1}{2}}}^{x_{k+\frac{1}{2}}} = 0$

2.4 Grouped Single Particle Model

Single Particle Model

The simplest discretized model assumes that there is only a single layer of solid particles in each electrode and that there is no electrolyte dynamics. Ignoring the electrolyte phase dynamics considerably reduces the system complexity and the number of model parameters. The resulting single particle model (SPM) is given by

$$\frac{\partial c_{s,i}}{\partial t} = \frac{1}{r^2}\frac{\partial}{\partial r}\left(D_{s,i} r^2 \frac{\partial c_{s,i}}{\partial r}\right), \tag{2.42}$$

$$\left.\frac{\partial c_{s,i}}{\partial r}\right|_{r=0} = 0, \quad \left. D_{s,i}\frac{\partial c_{s,i}}{\partial r}\right|_{r=R_{s,i}} = \pm\frac{I}{a_i L_i F A}, \tag{2.43}$$

$$\eta_{\mathrm{int},i} = \frac{2RT}{F}\sinh^{-1}\left(\frac{\pm I}{2k_i^{\mathrm{eff}} a_i L_i F A\sqrt{c_e^0\left(c_{s,i}^{\max} - c_i^{\mathrm{ss}}\right)c_i^{\mathrm{ss}}}}\right), \tag{2.44}$$

$$\mathrm{SOC}(t) = \mathrm{SOC}(0) - \frac{1}{Q}\int_0^t I(\tau)d\tau, \tag{2.45}$$

$$V = U_p(c_p^{\mathrm{ss}}) + \eta_p - U_n(c_n^{\mathrm{ss}}) - \eta_n, \tag{2.46}$$

$$\eta_{\mathrm{LiP}} = U_n(c_n^{\mathrm{ss}}) + \eta_n. \tag{2.47}$$

Note that here I is the input current in Amperes, defined as *positive* for *discharge*.

Single Particle Model With Grouped Parameters

The original SPM is still described with a large number of parameters. To further simplify the SPM for analysis of the influence of the parameters, a normalized, reformulated SPM with grouped parameters is introduced [14]. In the following equations, the index "s" indicating the solid phase and "int" indicating intercalation are omitted, as the SPM does not account for the electrolyte phase. A symbol with a bar denotes the normalized value of the

corresponding variable.

$$\frac{\partial \bar{c}_i}{\partial t} = \frac{1}{\theta'_{i1}} \frac{1}{\bar{r}_i^2} \frac{\partial}{\partial \bar{r}_i} \left(\bar{r}_i^2 \frac{\partial \bar{c}_i}{\partial \bar{r}_i} \right), \tag{2.48}$$

$$\left. \frac{\partial \bar{c}_i}{\partial \bar{r}_i} \right|_{\bar{r}_i=0} = 0, \left. \frac{\partial \bar{c}_i}{\partial \bar{r}_i} \right|_{\bar{r}_i=1} = -\theta'_{i2} I, \tag{2.49}$$

$$\eta_i = \frac{2RT}{F} \sinh^{-1} \left(\theta'_{i3} \frac{I}{\sqrt{\bar{c}_i^{\text{ss}} \left(1 - \bar{c}_i^{\text{ss}}\right)}} \right), \tag{2.50}$$

$$\text{SOC}(t) = \text{SOC}(0) - \frac{1}{Q} \int_0^t I(\tau) d\tau, \tag{2.51}$$

$$V = U_p(\bar{c}_p^{\text{ss}}) + \eta_p - U_n(\bar{c}_n^{\text{ss}}) - \eta_n, \tag{2.52}$$

$$\eta_{\text{LiP}} = U_n(\bar{c}_n^{\text{ss}}) + \eta_n. \tag{2.53}$$

where $\bar{r}_i = r/R_{s,i}$, $\bar{c}_i = c_i/c_{s,i}^{\max}$, $\bar{c}_i^{\text{ss}} = c_i^{\text{ss}}/c_{s,i}^{\max}$, and $i \in \{p, n\}$ represents the positive and negative electrodes.

The grouped parameters are defined as

$$\theta' = \begin{bmatrix} \theta'_{p1} \\ \theta'_{p2} \\ \theta'_{p3} \\ \theta'_{n1} \\ \theta'_{n2} \\ \theta'_{n3} \end{bmatrix} = \begin{bmatrix} \frac{R_p^2}{D_p} \\ -\frac{R_p^2}{D_p} \frac{1}{3\varepsilon_p L_p c_p^{\max} FA} \\ -\frac{R_p}{2k_p^{\text{eff}} \sqrt{c_e^0}} \frac{1}{3\varepsilon_p L_p c_p^{\max} FA} \\ \frac{R_n^2}{D_n} \\ \frac{R_n^2}{D_n} \frac{1}{3\varepsilon_n L_n c_n^{\max} FA} \\ \frac{R_n}{2k_n^{\text{eff}} \sqrt{c_e^0}} \frac{1}{3\varepsilon_n L_n c_n^{\max} FA} \end{bmatrix}, \tag{2.54}$$

with the meanings of the symbols given in Table 2.1.

The Padé approximation introduced in Section 2.3 can be applied to simplify the PDEs in the SPM [38], [39]. The normalized concentrations are now used to represent the lithium-ion concentration dynamics. With a 2nd-order Padé

approximation a reduced model for the concentration is

$$\frac{d\overline{c}_i^{\text{avg}}(t)}{dt} = -3\theta_{i2}I(t) \tag{2.55}$$

$$\frac{d\overline{c}_i^{\text{diff}}(t)}{dt} = -\frac{35}{\theta_{i1}}\overline{c}_i^{\text{diff}}(t) - 7\theta_{i2}I(t) \tag{2.56}$$

$$\overline{c}_i^{\text{ss}}(t) = \overline{c}_i^{\text{avg}}(t) + \overline{c}_i^{\text{diff}}(t), \tag{2.57}$$

where θ_{i1} and θ_{i2} are the redefined grouped parameters for the convenience of further analysis. With the knowledge of the initial averaged concentration $\overline{c}_i^{\text{avg}}(0)$ and assuming the initial $\overline{c}_i^{\text{diff}}(0) = 0$, (2.55)–(2.57) can be solved to give

$$\overline{c}_i^{\text{avg}}(t) = \overline{c}_i^{\text{avg}}(0) - 3\theta_{i2}\int_0^t I(t')dt' \tag{2.58}$$

$$\overline{c}_i^{\text{diff}}(t) = -\frac{I(t)\theta_{i1}\theta_{i2}}{5} + \frac{I(t)\theta_{i1}\theta_{i2}e^{\frac{-35t}{\theta_{i1}}}}{5} \tag{2.59}$$

$$\begin{aligned}\overline{c}_i^{\text{ss}}(t) = \overline{c}_i^{\text{avg}}(0) - 3\theta_{i2}\int_0^t I(t')dt' - \frac{I(t)\theta_{i1}\theta_{i2}}{5} \\ + \frac{I(t)\theta_{i1}\theta_{i2}e^{\frac{-35t}{\theta_{i1}}}}{5}.\end{aligned} \tag{2.60}$$

The negative overpotential is

$$\eta_n = \frac{2RT}{F}\sinh^{-1}\left(\theta_{n3}\frac{I}{\sqrt{\overline{c}_n^{\text{ss}}\left(1-\overline{c}_n^{\text{ss}}\right)}}\right), \tag{2.61}$$

and the new grouped parameters are

$$\theta = \begin{bmatrix}\theta_{p1}\\ \theta_{p2}\\ \theta_{p3}\\ \theta_{n1}\\ \theta_{n2}\\ \theta_{n3}\end{bmatrix} = \begin{bmatrix}\frac{R_p^2}{D_p}\\ -\frac{1}{3\varepsilon_p L_p c_p^{\max} FA}\\ -\frac{R_p}{2k_p^{\text{eff}}\sqrt{c_e^0}}\frac{1}{3\varepsilon_p L_p c_p^{\max} FA},\\ \frac{R_n^2}{D_n}\\ \frac{1}{3\varepsilon_n L_n c_n^{\max} FA}\\ \frac{R_n}{2k_n^{\text{eff}}\sqrt{c_e^0}}\frac{1}{3\varepsilon_n L_n c_n^{\max} FA}\end{bmatrix}. \tag{2.62}$$

CHAPTER 3

Methods

3.1 Parameter Sensitivity Analysis

The sensitivity analysis in this work relates to how much an output is affected by sensor errors and parameter uncertainties. Parameter sensitivity analysis is highly important for model identification, especially for complicated non-linear models such as the electrochemical lithium-ion battery model, which has a very large number of parameters. For such a complex kind of model, it is impossible to identify all the parameters without knowing the parameters' identifiability and correlation. A sensitivity analysis method is introduced to determine if a parameter can be identified or not. The more sensitive a parameter is, the higher the identifiability the parameter typically has. By performing sensitivity analysis a ranking and the correlation of the selected parameters' sensitivities can be deduced [40], [41]. Global sensitivity analysis is utilized to study the sensitivity of the parameters in their entire possible range, taking the nonlinearity of the system and the correlation between the parameters into account as well [19], [23]. To do such a global sensitivity analysis is computationally expensive, or even infeasible. Therefore, only a local sensitivity analysis is often performed to examine the sensitivity of a

complex system around a small vicinity of a specific parameter value set. In this work, a local sensitivity analysis is applied to the P2D model under various charging profiles and different model discretization orders. The parameter uncertainties, current sensor bias, and discretization errors are all considered in the analysis. In addition to the output voltage and temperature, the sensitivity of other important states is also analyzed, such as the lithium-plating overpotential and the growth of the SEI layer.

Among the large number of parameters in the lithium-ion battery electrochemical model, we exclude those that are constant, easy to obtain, or lack clear physical meaning. In total 23 parameters are selected for the later sensitivity analysis. The sensitivity can be different depending on the outputs and the initial state of the battery. Thus, for all selected parameters the same outputs and initial values are chosen for fair comparison of sensitivity. The selected parameters can be grouped into the following 4 categories:

1. Geometric parameters: $R_{s,p}$, L_p, $\varepsilon_{e,p}$, $\varepsilon_{s,p}$, $R_{s,n}$, L_n, $\varepsilon_{e,n}$, $\varepsilon_{s,n}$, L_{sep}, $\varepsilon_{e,sep}$, and A. These parameters describe the geometric characteristics of the battery, such as the thickness of the electrodes and the area of the electrode surface.

2. Transport parameters: $D_{s,p}$, σ_p, $D_{s,n}$, σ_n, D_e, t_+^0. These parameters describe the ions' transportation ability.

3. Kinetic parameters: k_p^{eff}, k_n^{eff}, brugg. These parameters describe the charge transfer ability.

4. Concentration parameters: $c_{s,p}^{\max}$, $c_{s,n}^{\max}$, c_e^0. They are the maximum solid-phase concentration in the two electrodes and the initial concentration in the electrolyte.

For a nonlinear system

$$y = f_\theta(u), \tag{3.1}$$

where $y \in \mathbb{R}^{n_y}$ is the vector of outputs, $u \in \mathbb{R}$ is the input and $\theta \in \mathbb{R}^{n_\theta}$ is the vector of parameters, the local sensitivity derivative vector $S_i \in \mathbb{R}^{n_y}$ of the model outputs to the i-th parameter is defined as

$$S_i = \left.\frac{\partial y}{\partial \theta_i}\right|_{\theta=\theta^*}, \tag{3.2}$$

where θ^* is the nominal parameter vector. However, S_i is usually numerically calculated from the response Δy to a parameter perturbation $\Delta\theta_i$, i.e.

$$\hat{S}_i = \left.\frac{\Delta y}{\Delta \theta_i}\right|_{\theta=\theta^*}. \tag{3.3}$$

The sensitivity derivative matrix $S \in \mathbb{R}^{n_y \times n_\theta}$ of the model outputs to the parameter vector is then defined as

$$\begin{aligned} S \equiv & \frac{\partial f_\theta}{\partial \theta}(u) \\ = & \left[\frac{\partial f_\theta}{\partial \theta_1}(u) \ \frac{\partial f_\theta}{\partial \theta_2}(u) \ \cdots \ \frac{\partial f_\theta}{\partial \theta_{n_\theta}}(u)\right] \\ \approx & \left[\hat{S}_1 \ \hat{S}_2 \ \cdots \ \hat{S}_{n_\theta}\right]. \end{aligned} \tag{3.4}$$

Since the P2D model is nonlinear, the value of S_i varies with θ^*. Despite this defect, this local sensitivity analysis method is useful as it has the advantage of being simple and computationally light. A set of nominal parameter values is chosen from experience, measurements and literature. Then a small uncertainty q_i is added to the i-th parameter, that is

$$\theta = [\theta_1, \theta_2, \cdots, \theta_i(1+q_i), \cdots, \theta_{n_\theta}],$$

followed by a new simulation run under the same conditions. In total, n_θ+1 simulations are needed for one input profile u. Here all the parameters have a unified uncertainty, that is all the uncertainties q_i have the same value. With this premise, two cases are studied. One assumes the uncertainty to be 0.5% while in the other case, it is assumed to be 2%. In other words, the N_θ simulations are repeated for $q_i = -0.5\%$, 0.5%, -2%, and 2%. By analyzing the simulation results, the rank of the parameter sensitivities for different outputs can be calculated.

3.2 Lithium-Plating Safety Margin

Grouped SPM-Inversion-Based Output Tracking Control Method

Charging the battery as quickly as possible, while not causing side reactions that lead to battery ageing is one of the key battery problems of today. Some widely used model-free charging methods, such as CV (Constant Voltage), CP (Constant Power), CCCV (Constant Current Constant Voltage) can limit the voltage, current, or power while charging, but the dynamics of the internal conditions in the battery are ignored. Under these circumstances, increasing the charging C-rate for faster charging without caring about the battery's inner states can cause severe degradation and even be dangerous. To realize health-conscious fast charging, electrochemical model-based charging methods are introduced. Considering the complexity of the electrochemical model, some feedback control methods like MPC or PID control where control parameters need to be tuned are hard to apply in practice. Also, the optimisation strategies can be very time-consuming when searching for a globally optimised solution. Inversion-based model output tracking control method has been introduced to calculate the optimal solution at each time instant directly from the tracking goals. One of the main disadvantages of this method is that it requires a high model accuracy. However, as mentioned previously, it is hard to get the exact values of many of the parameters in the lithium-ion battery electrochemical model, especially when considering the degradation of the batteries, since this continuously changes many of the parameters. As a consequence, it is important to have a safety margin when operating the inversion-based control, to avoid violating the constraints set up for the charging [15].

Here we will only focus on the constraint set to avoid lithium plating, i.e. keeping the lithium plating overpotential positive during fast charging, which can be expressed as

$$\eta_{\text{LiP}} = U_n(\overline{c}_n^{\text{ss}}) + \eta_n = \eta_{\min} \geq 0, \tag{3.5}$$

where $\eta_{\min}$ is introduced as a safety margin the controller aims to track.

Combining (3.5) with (2.61), the control current can be calculated as

$$I = \sinh\left((\eta_{\min} - U_n(\bar{c}_n^{\text{ss}}))\frac{F}{2RT}\right)\frac{\sqrt{\bar{c}_n^{\text{ss}}(1-\bar{c}_n^{\text{ss}})}}{\theta_{n3}}, \tag{3.6}$$

which should give a Li-plating overpotential equal to $\eta_{\min}$, in theory. In the beginning of the charging the calculated current is too large for the hardware to apply. Therefore, a limitation I_c is set to restrict the applied current before the model-inversion-based control is triggered. The calculated input current in (3.6) will only be adopted when it is smaller than the limit I_c. In other words, the final applied input current is

$$I_{\text{app}} = \min(|I|, |I_c|), \tag{3.7}$$

where I is calculated from (3.6).

Constant Safety Margin

In the SPM-inversion-based output tracking control method, the accuracy of the parameters plays an important role. The control current is calculated based on the model parameters and the model states. With inaccurate parameters, the control current can lead to Li-plating being smaller than its safety margin $\eta_{\min}$. If $\eta_{\min}$ is chosen to be inappropriately small, such that the Li-plating overpotential actually goes below zero, Li-plating will happen and potentially cause serious battery degradation. Simply choosing a large safety margin to prevent the Li-plating from happening will extend the charging time a lot. In order to shorten the charging time as much as possible a minimum safety margin should be applied.

Assume the model parameters are restricted within a range decided by q_i, i.e.

$$\theta_i = (1 + q_i)\hat{\theta}_i, \quad i = 1, 2, 3, ... \tag{3.8}$$

where θ_i is the grouped plant parameters, $\hat{\theta}_i$ is the grouped model parameters and q_i is the normalised difference between the i-th plant parameter and the corresponding model parameter.

Denote

$$\hat{U}_n = F_n(\hat{\bar{c}}_n)$$
$$U_n = F_n(\bar{c}_n)$$
$$\Delta\bar{c}_n = \hat{\bar{c}}_n - \bar{c}_n.$$

Applying a first-order Taylor expansion, we have

$$F_n(\bar{c}_n) = F_n(\hat{\bar{c}}_n) + F_n'(\hat{\bar{c}}_n)(\bar{c}_n - \hat{\bar{c}}_n), \tag{3.9}$$

and

$$U_n = \hat{U}_n - F_n'(\hat{\bar{c}}_n)\Delta\bar{c}_n = \hat{U}_n + \Delta_{n1}, \tag{3.10}$$

where

$$\Delta_{n1} = -F_n'(\hat{\bar{c}}_n)\Delta\bar{c}_n. \tag{3.11}$$

Similarly, denote

$$\hat{\eta}_n = Y_n(\hat{\bar{c}}_n, \hat{\theta}_{n3})$$
$$\eta_n = Y_n(\bar{c}_n, \theta_{n3})$$
$$\Delta\theta_{n3} = \hat{\theta}_{n3} - \theta_{n3} = -q_{n3}\hat{\theta}_{n3}.$$

Once more, using a first-order Taylor expansion,

$$\begin{aligned} Y_n(\bar{c}_n, \theta_{n3}) &= Y_n(\hat{\bar{c}}_n, \hat{\theta}_{n3}) + Y'_{n,\hat{\bar{c}}_n}(\hat{\bar{c}}_n, \hat{\theta}_{n3})(\bar{c}_n - \hat{\bar{c}}_n) \\ &\quad + Y'_{n,\hat{\theta}_{n3}}(\hat{\bar{c}}_n, \hat{\theta}_{n3})(\theta_{n3} - \hat{\theta}_{n3}) \qquad (3.12) \\ \eta_n &= \hat{\eta}_n - Y'_{n,\hat{\bar{c}}_n}(\hat{\bar{c}}_n, \hat{\theta}_{n3})\Delta\bar{c}_n - Y'_{n,\hat{\theta}_{n3}}(\hat{\bar{c}}_n, \hat{\theta}_{n3})\Delta\theta_{n3} \\ &= \hat{\eta}_n + \Delta_{n2}, \qquad (3.13) \end{aligned}$$

where

$$\Delta_{n2} = -Y'_{n,\hat{\bar{c}}_n}(\hat{\bar{c}}_n, \hat{\theta}_{n3})\Delta\bar{c}_n - Y'_{n,\hat{\theta}_{n3}}(\hat{\bar{c}}_n, \hat{\theta}_{n3})\Delta\theta_{n3}. \tag{3.14}$$

With Δ_{n2} and Δ_{n1}, the relationship between $\hat{\eta}_{\text{LiP}}$ and η_{LiP}, can be expressed as

$$\begin{aligned} \eta_{\text{LiP}} &= U_n + \eta_n \\ &= (\hat{U}_n + \Delta_{n1}) + (\hat{\eta}_n + \Delta_{n2}) \qquad (3.15) \\ &= \hat{\eta}_{\text{LiP}} + \Delta_{n1} + \Delta_{n2}. \end{aligned}$$

Now, let $\hat{\eta}_{\text{LiP}} = \hat{\eta}_{\min}$ and $\eta_{\text{LiP}} = \eta_{\min}$, which gives

$$\hat{\eta}_{\min} = \eta_{\min} - \Delta_{n1} - \Delta_{n2}. \tag{3.16}$$

Equation (3.16) suggests that in order to achieve lithium-plating-free charging control, i.e., $\eta_{\min} = 0$, the safety margin should be set to $-(\Delta_{n1} + \Delta_{n2})$. Consequently, denote the safety margin as

$$\eta_{\text{safem}} = -\Delta_{n1} - \Delta_{n2}. \tag{3.17}$$

The range of the bias can be available in practice [14], [42]. In this case, the minimum safety margin can be found so that no combination of parameter biases can lead to lithium plating during the charging process.
Assuming $-1 < q_{ni} < 1,\ i = 1, 2, 3$, it can be derived that

$$\begin{aligned}
\frac{\partial \Delta \bar{c}_n}{\partial q_{n1}} &= \frac{I(t)}{5} \hat{\theta}_{n1} \hat{\theta}_{n2} (1 + q_{n2}) < 0 \\
\frac{\partial \Delta \bar{c}_n}{\partial q_{n2}} &= 3\hat{\theta}_{n2} \int_0^t I(t')dt' + \frac{I(t)}{5} \hat{\theta}_{n1} \hat{\theta}_{n2} (1 + q_{n1}) < 0 \\
\frac{\partial \Delta_{n1}}{\partial q_i} &= \frac{d\Delta_{n1}}{d\Delta \bar{c}_n} \frac{\partial \Delta \bar{c}_n}{\partial q_i} = -F_n'(\hat{\bar{c}}_n) \frac{\partial \Delta \bar{c}_n}{\partial q_i}, i \in \{n1, n2\} \\
\frac{\partial \Delta_{n2}}{\partial q_i} &= \frac{\partial \Delta_{n2}}{\partial \Delta \bar{c}_n} \frac{\partial \Delta \bar{c}_n}{\partial q_i} \\
&= -Y'_{n,\hat{\bar{c}}_n}(\hat{\bar{c}}_n, \hat{\theta}_{n3}) \frac{\partial \Delta \bar{c}_n}{\partial q_i}, i \in \{n1, n2\} \\
\frac{\partial \Delta_{n2}}{\partial q_{n3}} &= \frac{\partial \Delta_{n2}}{\partial \Delta \theta_{n3}} \frac{\partial \Delta \theta_{n3}}{\partial q_{n3}} = Y'_{n,\hat{\theta}_{n3}}(\hat{\bar{c}}_n, \hat{\theta}_{n3}) \hat{\theta}_{n3}.
\end{aligned} \tag{3.18}$$

Combining the derivatives above with the knowledge of the range of the grouped parameter biases it is possible to calculate the minimum constant safety margin preventing Li-plating. The safety margin is then selected as the largest value of the time series η_{safem}. The whole process is described in Algorithm 1.

Algorithm 1 Find the safety margin with known parameter bias values

Input $tol = 1 \times 10^{-9}$, $\eta_{\min} = 0$, $\hat{\theta}_i$, $\hat{q}_i$, and I_c
Output $\hat{\eta}_{\min}$ and I_{app}

Initialize $\hat{\eta}_{\min} = \eta_{\min} - 0.1$;
for each iteration **do**
    $\hat{\eta}_{\min}^{\text{pre}} = \hat{\eta}_{\min}$
    for each time sample **do**
        Calculate model-inversion-based current
        $\hat{I} = f(\hat{\eta}_{\min})$,
        $I_{\text{app}} = \max(|I_c|, |\hat{I}|)$
    end for
    Calculate time-dependent $\hat{\eta}_{\min}(t)$ series by (3.11), (3.14), and (3.16);
    $\hat{\eta}_{\min} = \max(\hat{\eta}_{\min}(t_{\text{inv}} : t_{\text{end}}))$, where t_{inv} is the time when $\hat{I}$ starts to be effective;
    if $\|\hat{\eta}_{\min}^{\text{pre}} - \hat{\eta}_{\min}\|_\infty < tol$ **then**
        break
    end if
end for

Calculated the Dynamic Safety Margin

The constant safety margin is chosen from the maximum value in the safety margin time series after the inversion-based control starts according to Algorithm 1. However, the charging time can become very long when using the constant safety margin, since most of the time the required safety margin is smaller than the chosen value. To reduce the total charging time we therefore allow the safety margin to vary in time, though still guaranteeing no lithium plating as long as the parameters stay within the specified bounds.

According to the previous analysis in Chapter 3.2, we define the worst model as the one with the parameter biases that lead to the maximum safety margin η_{safem}. The relationship between the worst model and the original model parameters is

$$\theta_{w,ik} = (1 + q_{w,ik})\hat{\theta}_{ik}, \quad i \in \{p, n\},\ k = 1, 2, 3, \tag{3.19}$$

where $q_{w,ik}$ is the bias between the worst model and the original model pa-

rameter.

It can be proven (see Paper C) that for a fixed q_w, the dynamic safety margin is only SOC dependent and can be calculated. The optimal control current can then be calculated from

$$\hat{I}_w(t) = \sinh\left((\hat{\eta}_{w,min} - \hat{U}_{w,n})\frac{F}{2RT}\right)\frac{\sqrt{\hat{\bar{c}}^{\text{ss}}_{w,n}(t)(1-\hat{\bar{c}}^{\text{ss}}_{w,n}(t))}}{\theta_{n3}}, \tag{3.20}$$

where $\hat{\eta}_{w,min} = 0$, $\hat{U}_{w,n}$ and $\hat{\bar{c}}^{\text{ss}}_{w,n}$ are the worst model states. With the above analysis, an online Li-plating free fast charging process can be described as in Fig. 3.1.

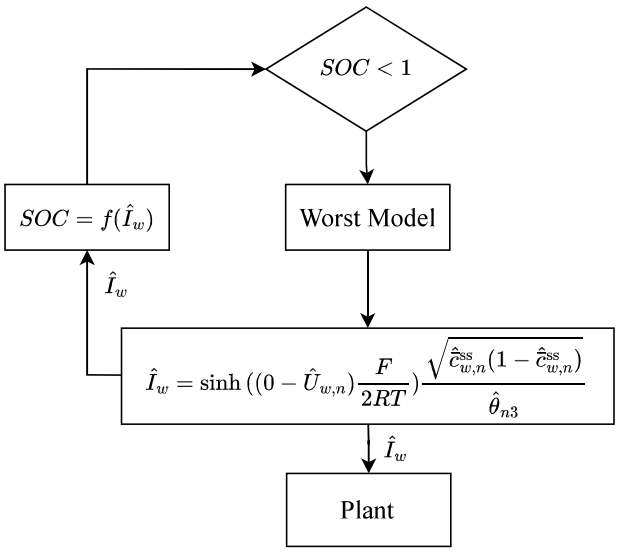

Figure 3.1: Online charging process with the worst-case model and dynamic safety margin

In addition, the voltage difference between the model terminal voltage and the plant terminal voltage can be approximated by a linear combination of the biases q between the model and the plant according to

$$\Delta V_{bat}(t) = \hat{V}_{bat}(t) - V_{bat}(t) \approx Hq, \tag{3.21}$$

where

$$H = \begin{bmatrix} H_{p1} & H_{p2} & H_{p3} & H_{n1} & H_{n2} & H_{n3} \end{bmatrix} \tag{3.22}$$

can be easily calculated at each time instant and

$$q = \begin{bmatrix} q_{p1} & q_{p2} & q_{p3} & q_{n1} & q_{n2} & q_{n3} \end{bmatrix}^T \tag{3.23}$$

With this approximation, a recursive least square (RLS) parameter identification part can be applied to identify the vector q and hence the plant parameters. Using this identification, the bias ranges can be narrowed, and a faster charging can thus be realized. The charging process with the RLS parameter identification part is illustrated in Fig.3.2

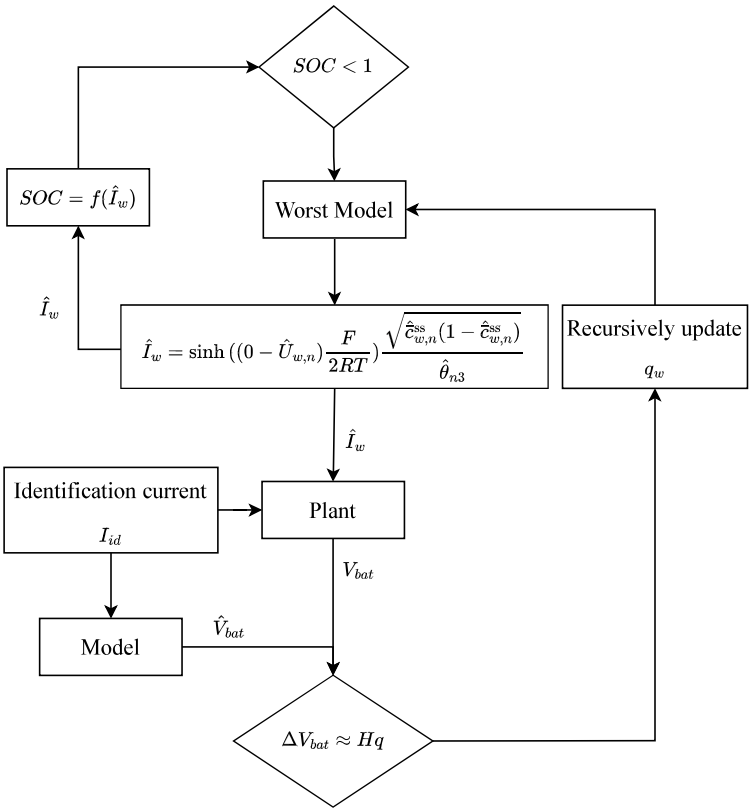

Figure 3.2: Online charging process with the worst-case model, dynamic safety margin and parameter identification

CHAPTER 4

Summary of included papers

This chapter provides a summary of the included papers.

4.1 Paper A

Yao Cai, Changfu Zou, Yang Li, and Torsten Wik
Fast Charging Control of Lithium-Ion Batteries: Effects of Input, Model, and Parameter Uncertainties
Published in 2022 European Control Conference (ECC),
pp. 1647–1653, July 2022.
 DOI: 10.23919/ECC55457.2022.9838024 .

This work aims to pinpoint the minimum model complexity for health-conscious fast charging control of lithium-ion batteries in the presence of sensor biases and parameter errors. Starting from a high-fidelity physics-based model that describes both the normal intercalation reaction and the dominant side reactions, Padé approximation and the finite volume method are employed for model simplification, with the number of control volumes as a tuning parameter. A P2D model is implemented and the errors of the selected outputs

with different orders of the model are investigated under the HPPC profile. With this analysis, for given requirements on modelling accuracy, extensive model-based simulations are conducted to find the simplest models, based on which the effects of current sensor bias and parameter errors are systematically studied. To do this, simulations are performed to find the absolute errors of the lithium plating potential under different current biases. Two cases are studied, one assumes the uncertainty to be 0.5% while the other one assumes it to be 2%. A sensitivity analysis is done to study the effects of the parameter errors, and the analysis is based on the P2D model and for various charging profiles. A set of nominal parameters is selected from the P2D model and their values are decided from experience and literature. Then a small uncertainty is added to each parameter, one at a time. The results show that relatively low-order models can be well-qualified for controlling voltage, state of charge, and temperature. On the other hand, high-order models are necessary for health management, particularly during fast charging, and the choice of the safety margin should also consider the current sensor biases. Furthermore, increasing the model order will not improve model accuracy unless the parameters are sufficiently accurate.

4.2 Paper B

Yao Cai, Yang Li, Torsten Wik
Safety Margin for Li-Plating Free Fast-Charging of Li-Ion Batteries Considering Parameter Uncertainty
Accepted in 8th IEEE Conference on Control Technology and Applications (CCTA) Newcastle upon Tyne, , 2024-08-21 - 2024-08-23 .

In this work, an algorithm that realizes the Li-plating-free fast-charging of Li-ion batteries considering the parameter uncertainties is proposed. Fast charging of the lithium-ion battery is key to deal with range anxiety. However, there is always a contradiction between a higher charging rate and a longer battery life, since some side reactions can be caused by a too high charging rate, such as Li-plating, SEI growth and particle cracking. How to charge as fast as possible while not leading to excessive ageing has therefore become an important research topic. This paper introduces a single particle model-based inversion-based fast charging method with a calculated safety margin, and a grouped SPM is used for analysis. One disadvantage of the inversion-

based fast-charging method is that it relies a lot on the accuracy of the model parameters that cannot be identified precisely due to inevitable differences between the model and the plant. To deal with this problem, the proposed algorithm can calculate a theoretical Li-plating safety margin based on the provided range of parameter uncertainties. The simulations and theoretical analysis show that with this safety margin, lithium plating can be completely avoided provided the battery can be accurately described by the model for some parameter setting within the specified intervals.

4.3 Paper C

Yao Cai, Yang Li, Torsten Wik
Dynamic Safety Margin with Parameter Identification for Li-Plating-Free Fast-Charging of Li-Ion Batteries
Manuscript for submission, July 2024 .

In this work, an analytical calculation of a minimum dynamic safety margin for non-Li-plating fast charging from the ranges of parameter biases is provided. Also here the derivations are based on a grouped single particle model (SPM) based inversion control method. It is shown that the optimal current as well as the dynamic safety margin for the plating overpotential depends only on the SOC and the specified parameter ranges. Instead of a constant safety margin, from experience or from calculation, the dynamic safety margin introduced here can accelerate the charging process significantly. Furthermore, it is shown that at each time instant the difference between the measured voltage and the modelled voltage can be approximated by a known linear combination of the parameter biases. These can then be estimated using recursive least squares, which reduces the ranges of the parameter biases and can thus reduce the required charging time for Li-plating-free fast-charging even further.

CHAPTER 5

Conclusions and Future Work

Conclusions

The health-aware fast charging of lithium-ion batteries is an essential topic for the development of electric vehicles. To address the goal of ultra-fast charging, a well-identified battery model is needed. The identifiability of the parameters can be assessed by a sensitivity analysis. In this thesis, a local sensitivity analysis w.r.t. 23 parameters in a P2D model is introduced. In addition to parameter uncertainties, the current sensor bias and discretization errors are also considered in the sensitivity analysis. In addition to the output voltage, temperature, state of charge (SOC), and state of health (SOH), two degradation-related states, the lithium-plating overpotential and the growth of the SEI layer, are taken into consideration. The results indicate that the higher the model order is, the more accurate the simulation results tend to be. However, depending on the parameter uncertainties there is a quite low limit for how high order of the discretized model that is meaningful.

To compensate for the effects of the parameter uncertainties when aiming for Li-plating-free fast charging, a method for analytically calculating the

required safety margin is introduced. Provided that the ranges of the parameter biases are known when performing SPM-inversion-based fast charging, the derivatives of the safety margin with respect to the parameter biases can be calculated. With this information, the bias combination that leads to the maximum required safety margin series in the given parameter range can be found. The maximum value in this series is thus the minimum constant safety margin that can prevent any Li-plating from happening within the given parameter biases range.

However, this calculated constant safety margin is often unnecessarily large for most parts of the charging process. Charging time can be reduced by selecting a smaller safety margin when possible. Therefore, a dynamic safety margin is introduced for ultra-fast charging. Still based on the SPM-inversion-based fast charging, and using the information on safety margin derivatives with respect to parameter biases, a unique safety margin can be determined for each control time constant. This approach significantly reduces charging time and enables the fastest Li-plating-free charging within the range of parameter uncertainties (biases). Furthermore, an approximate linear regression with the biases as unknown parameters is derived. By applying recursive least squares, the parameter biases can be identified, which reduces the ranges of the parameter biases and further shortens the required charging time for Li-plating-free fast charging.

Future Work

Since the P2D model offers superior performance in predicting ageing-related states compared to the SPM, applying a similar method to calculate the analytical dynamic safety margin based on P2D model-inversion-based control is a highly interesting topic for further research. The main obstacle is that the P2D model has many more parameters than the grouped SPM investigated in this thesis, which makes it more difficult to calculate the derivatives of the safety margin with respect to the parameters' biases, which is vital to the analysis.

Moreover, the linear regression with the biases as unknown parameters based on recursive least squares can be verified using the P2D model. The

P2D model can then serve as a plant for parameter identification, allowing the generation of data for fitting the parameters of the SPM. After this, the Li-plating free SPM-inversion-based fast charging protocol can be designed and then tested on a P2D model. Ultimately, of course, we need to test the methods experimentally in the battery lab. Other methods than recursive least squares as well as input design methods for identification can also be interesting to apply to the linear regression for improved identification results.

References

[1] P. Plötz, J. Wachsmuth, T. Gnann, F. Neuner, D. Speth, and S. Link, "Net-zero-carbon transport in europe until 2050—targets, technologies and policies for a long-term EU strategy," *Karlsruhe: Fraunhofer Institute for Systems and Innovation Research ISI*, 2021.

[2] M. Wu and W. Chen, "Forecast of electric vehicle sales in the world and china based on PCA-GRNN," *Sustainability*, vol. 14, no. 4, 2022.

[3] W. Li, D. Cao, D. Jöst, *et al.*, "Parameter sensitivity analysis of electrochemical model-based battery management systems for lithium-ion batteries," *Appl. Energy*, vol. 269, p. 115 104, 2020.

[4] Y. Li, M. Vilathgamuwa, T. Farrell, S. S. Choi, N. T. Tran, and J. Teague, "A physics-based distributed-parameter equivalent circuit model for lithium-ion batteries," *Electrochim. Acta*, vol. 299, pp. 451–469, 2019.

[5] K. W. E. Cheng, B. P. Divakar, H. Wu, K. Ding, and H. F. Ho, "Battery-management system (BMS) and SOC development for electrical vehicles," *IEEE Trans. Veh. Technol.*, vol. 60, no. 1, pp. 76–88, 2011.

[6] M. Nizam, H. Maghfiroh, R. A. Rosadi, and K. D. Kusumaputri, "Battery management system design (BMS) for lithium ion batteries," in *AIP Conf. Proc.*, AIP Publishing, vol. 2217, 2020.

[7] M.-K. Tran, A. Mevawala, S. Panchal, K. Raahemifar, M. Fowler, and R. Fraser, "Effect of integrating the hysteresis component to the equivalent circuit model of lithium-ion battery for dynamic and non-dynamic applications," *J. Energy Storage*, vol. 32, p. 101 785, 2020.

[8] Y. Li, Z. Wei, B. Xiong, and D. M. Vilathgamuwa, "Adaptive ensemble-based electrochemical–thermal degradation state estimation of lithium-ion batteries," *IEEE Trans. Ind. Electron.*, vol. 69, no. 7, pp. 6984–6996, 2022.

[9] Y. Li, D. M. Vilathgamuwa, E. Wikner, *et al.*, "Electrochemical model-based fast charging: Physical constraint-triggered PI control," *IEEE Trans. Energy Convers.*, vol. 36, no. 4, pp. 3208–3220, 2021.

[10] Z. Chu, X. Feng, L. Lu, J. Li, X. Han, and M. Ouyang, "Non-destructive fast charging algorithm of lithium-ion batteries based on the control-oriented electrochemical model," *Appl. Energy*, vol. 204, pp. 1240–1250, 2017.

[11] Y. Li, B. Xiong, D. M. Vilathgamuwa, Z. Wei, C. Xie, and C. Zou, "Constrained ensemble Kalman filter for distributed electrochemical state estimation of lithium-ion batteries," *IEEE Trans. Ind. Inform.*, vol. 17, no. 1, pp. 240–250, 2021.

[12] C. Li, N. Cui, C. Wang, and C. Zhang, "Reduced-order electrochemical model for lithium-ion battery with domain decomposition and polynomial approximation methods," *Energy*, vol. 221, p. 119 662, 2021.

[13] Z. Deng, H. Deng, L. Yang, Y. Cai, and X. Zhao, "Implementation of reduced-order physics-based model and multi-parameters identification strategy for lithium-ion battery," *Energy*, vol. 138, pp. 509–519, 2017.

[14] A. M. Bizeray, J.-H. Kim, S. R. Duncan, and D. A. Howey, "Identifiability and parameter estimation of the single particle lithium-ion battery model," *IEEE Trans. Control Syst. Technol.*, vol. 27, no. 5, pp. 1862–1877, 2019.

[15] Y. Li, T. Wik, Y. Huang, and C. Zou, "Nonlinear model inversion-based output tracking control for battery fast charging," *IEEE Trans. Control Syst. Technol.*, vol. 32, no. 1, pp. 225–240, 2024.

[16] N. Ghaeminezhad and M. Monfared, "Charging control strategies for lithium-ion battery packs: Review and recent developments," *IET Power Electron.*, vol. 15, no. 5, pp. 349–367, 2022.

[17] A. Pozzi, M. Torchio, R. D. Braatz, and D. M. Raimondo, "Optimal charging of an electric vehicle battery pack: A real-time sensitivity-based model predictive control approach," *J. Power Sources*, vol. 461, p. 228 133, 2020.

[18] S. Kolluri, S. V. Aduru, M. Pathak, R. D. Braatz, and V. R. Subramanian, "Real-time nonlinear model predictive control (NMPC) strategies using physics-based models for advanced lithium-ion battery management system (BMS)," *J. Electrochem. Soc.*, vol. 167, no. 6, p. 063 505, 2020.

[19] M. Streb, M. Ohrelius, M. Klett, and G. Lindbergh, "Improving Li-ion battery parameter estimation by global optimal experiment design," *J. Energy Storage*, vol. 56, p. 105 948, 2022.

[20] V. Laue, F. Röder, and U. Krewer, "Practical identifiability of electrochemical P2D models for lithium-ion batteries," *J. Appl. Electrochem.*, vol. 51, no. 9, pp. 1253–1265, 2021.

[21] M. Andersson, M. Streb, J. Y. Ko, *et al.*, "Parametrization of physics-based battery models from input–output data: A review of methodology and current research," *J. Power Sources*, vol. 521, p. 230 859, 2022.

[22] C. Edouard, M. Petit, C. Forgez, J. Bernard, and R. Revel, "Parameter sensitivity analysis of a simplified electrochemical and thermal model for Li-ion batteries aging," *J. Power Sources*, vol. 325, pp. 482–494, 2016.

[23] M. Streb, M. Andersson, V. Löfqvist Klass, M. Klett, M. Johansson, and G. Lindbergh, "Investigating re-parametrization of electrochemical model-based battery management using real-world driving data," *eTransport.*, vol. 16, p. 100 231, 2023.

[24] G. L. Plett, *Battery Management Systems, Volume I: Battery Modeling.* Artech House, 2015.

[25] A. Jokar, B. Rajabloo, M. Désilets, and M. Lacroix, "Review of simplified pseudo-two-dimensional models of lithium-ion batteries," *J. Power Sources*, vol. 327, pp. 44–55, 2016.

[26] A. Tomaszewska, Z. Chu, X. Feng, *et al.*, "Lithium-ion battery fast charging: A review," *eTransport.*, vol. 1, p. 100 011, 2019.

[27] J. S. Edge, S. O'Kane, R. Prosser, *et al.*, "Lithium ion battery degradation: What you need to know," *Phys. Chem. Chem. Phys.*, vol. 23, no. 14, pp. 8200–8221, 2021.

[28] R. Nemes, S. Ciornei, M. Ruba, H. Hedesiu, and C. Martis, "Modeling and simulation of first-order Li-ion battery cell with experimental validation," in *2019 8th Int. Conf. Modern Power Syst. (MPS)*, 2019, pp. 1–6.

[29] M. Dubarry, N. Vuillaume, and B. Y. Liaw, "From single cell model to battery pack simulation for Li-ion batteries," *J. Power Sources*, vol. 186, no. 2, pp. 500–507, 2009.

[30] M. Doyle, T. F. Fuller, and J. Newman, "Modeling of galvanostatic charge and discharge of the lithium/polymer/insertion cell," *J. Electrochem. Soc.*, vol. 140, no. 6, p. 1526, Jun. 1993.

[31] T. F. Fuller, M. Doyle, and J. Newman, "Simulation and optimization of the dual lithium ion insertion cell," *J. Electrochem. Soc.*, vol. 141, no. 1, p. 1, Jan. 1994.

[32] M. Torchio, L. Magni, R. B. Gopaluni, R. D. Braatz, and D. M. Raimondo, "LIONSIMBA: A Matlab framework based on a finite volume model suitable for Li-ion battery design, simulation, and control," *J. Electrochem. Soc.*, vol. 163, 2016.

[33] X.-G. Yang, Y. Leng, G. Zhang, S. Ge, and C.-Y. Wang, "Modeling of lithium plating induced aging of lithium-ion batteries: Transition from linear to nonlinear aging," *J. Power Sources*, vol. 360, pp. 28–40, 2017.

[34] N. A. Chaturvedi, R. Klein, J. Christensen, J. Ahmed, and A. Kojic, "Algorithms for advanced battery-management systems," *IEEE Control Syst. Mag.*, vol. 30, no. 3, pp. 49–68, 2010.

[35] Y. Li, D. Karunathilake, D. M. Vilathgamuwa, *et al.*, "Model order reduction techniques for physics-based lithium-ion battery management: A survey," *IEEE Ind. Electron. Mag.*, vol. 16, no. 3, pp. 36–51, 2022.

[36] V. R. Subramanian, V. D. Diwakar, and D. Tapriyal, "Efficient macro-micro scale coupled modeling of batteries," *J. Electrochem. Soc.*, vol. 152, no. 10, A2002, Aug. 2005.

[37] J. H. Summerfield and C. N. Curtis, "Modeling the lithium ion/electrode battery interface using fick's second law of diffusion, the laplace transform, charge transfer functions, and a [4, 4] padé approximant," *International Journal of Electrochemistry*, vol. 2015, no. 1, p. 496 905, 2015.

[38] N. T. Tran, M. Vilathgamuwa, T. Farrell, S. S. Choi, Y. Li, and J. Teague, "A Padé approximate model of lithium ion batteries," *J. Electrochem. Soc.*, vol. 165, no. 7, A1409, May 2018.

[39] J. Basdevant, "The Padé approximation and its physical applications," *Fortschritte der Physik*, vol. 20, no. 5, pp. 283–331, 1972.

[40] J. Li, L. Zou, F. Tian, X. Dong, Z. Zou, and H. Yang, "Parameter identification of lithium-ion batteries model to predict discharge behaviors using heuristic algorithm," *J. Electrochem. Soc.*, vol. 163, no. 8, A1646, Jun. 2016.

[41] M. Lagnoni, C. Nicolella, and A. Bertei, "Survey and sensitivity analysis of critical parameters in lithium-ion battery thermo-electrochemical modeling," *Electrochim. Acta*, vol. 394, p. 139 098, 2021.

[42] E. Namor, D. Torregrossa, R. Cherkaoui, and M. Paolone, "Parameter identification of a lithium-ion cell single-particle model through non-invasive testing," *J. Energy Storage*, vol. 12, pp. 138–148, 2017.